Understanding the Bandwidth Limitations in Monolithic 1.3 μm InAs/GaAs Quantum Dot Lasers on Silicon

Constanze Hantschmann, Peter P. Vasil'ev, Adrian Wonfor, *Member, IEEE,* Siming Chen, *Member, IEEE,* Mengya Liao, *Student Member, IEEE,* Alwyn J. Seeds, *Fellow, IEEE,* Huiyun Liu, *Senior Member, IEEE,* Richard V. Penty, *Senior Member, IEEE,* and Ian H. White, *Fellow, IEEE*

***Abstract*— In this paper, we present measurements and simulations of the small-signal modulation response of monolithic continuous-wave 1.3 μm InAs/GaAs quantum dot (QD) narrow ridge-waveguide lasers on a silicon substrate. The 2.5 mm-long lasers investigated demonstrate 3dB modulation bandwidths of 1.6 GHz, *D*-factors of 0.3 GHz/mA$^{1/2}$, modulation current efficiencies of 0.4 GHz/mA$^{1/2}$, and *K*-factors of 2.4 ns and 3.7 ns. Since the devices under test are not designed for high-speed operation due to their long length and hence long photon lifetime, the modulation response curves are used as a fitting template for numerical simulations with spatiotemporal resolution to gain insight into the underlying laser physics. The obtained parameter set is used to unveil the true potential of the laser material in an optimized device geometry by modeling the small-signal response at different cavity lengths, mirror reflectivities, and for different numbers of QD layers. The simulations predict a maximum 3dB modulation bandwidth of 5 GHz to 7 GHz for a 0.75 mm-long cavity with 99 % and 60 % high-reflection coatings and ten QD layers. Modeling the impact of dislocations on the dynamic performance qualitatively reveals that enhanced non-radiative recombination in the wetting layer leaves the modulation bandwidth of QD lasers on silicon almost unaffected, while dislocation-induced optical loss does not pose a problem, as long as sufficient gain is provided by the QD active region.**

***Index Terms*— Integrated optics, modulation, quantum dot lasers, semiconductor device modeling, silicon devices**

I. Introduction

BANDWIDTH-THIRSTY web-based applications, such as cloud storage, social networking, and streaming services, have drastically shaped the development of the data communication landscape, and are expected to require even more capacity in the coming years [1]. To address this issue, silicon (Si) photonics-enabled processors hold great potential for next generation data centers and high-performance computers, driven by the benefits of high integration densities and lower power consumption alongside reduced cost enabled by CMOS-compatible large-scale fabrication [1], [2].

The first realization of 1.3 μm continuous-wave (cw) room temperature GaAs-based lasers with InAs quantum dot (QD) active regions directly grown on Si was, therefore, a considerable technological breakthrough [3]. By now, the continuous optimization of these devices through dislocation filter layers, thermal cyclic annealing, and GaP buffer layers [4] has led to cw characteristics that are comparable with InAs QD lasers on their native substrate [3], [5]-[8]. *Jung et al.*, for example, have recently reported a low threshold current of 6.2 mA, high optical output power of 185 mA, and a record lifetime of more than one million hours [7], thus clearly proving that QD lasers on Si substrates are well on the way to address the demand for cw on-chip light sources [2].

Yet even without the benefits of optoelectronic integration, QD lasers on Si have a compelling advantage over III/V lasers on native substrates with respect to the significantly reduced fabrication cost when growing on inexpensive large-area Si wafers [8]. Backed by the low linewidth enhancement factor typical for QD lasers [9] and Si's favourable heat dissipation properties [8], this means that Si-based QD lasers could become truly competitive low-cost transmitters for direct modulation applications. There is, however, reason to believe that the dynamic characteristics of these devices are inherently impaired by the QDs' modulation properties: QD lasers suffer typically from limited modal gain [10], a high gain saturation factor inducing strong damping to the small-signal response, and longer time constants due to cascaded carrier transport [11]. Although there are also 10 Gb/s × 10 lane architectures requiring lower modulation bandwidth being deployed in data centers, directly or externally modulated 4 × 25 Gb/s solutions may perhaps be more viable for reasons of system complexity and cost per square millimeter [12], [13]. Additionally, the ever-increasing bandwidth consumption also drives the demand

Manuscript received August 28 2018. This work is supported by UK EPSRC at the University of Cambridge and at University College London (UCL Grant No. EP/J012904/1 and EP/J012815/1). C. Hantschmann's Ph.D. studies are funded by Qualcomm Inc.. S.-M. Chen's Research Fellowship is funded by the Royal Academy of Engineering under Reference No. RF201617/16/28.

C. Hantschmann, P. P. Vasil'ev, A. Wonfor, R. V. Penty, and I. H. White are with the Centre for Photonic Systems, Department of Engineering, University of Cambridge, Cambridge CB3 0FA, UK. (e-mail: cb893@cam.ac.uk; pv261@cam.ac.uk, aw300@cam.ac.uk, rvp11@cam.ac.uk, ihw3@cam.ac.uk).

S.-M. Chen, M. Liao, A. J. Seeds, and H. Liu are with the Department of Electronic and Electrical Engineering, University College London, London WC1E 7JE, UK. (e-mail: siming.chen@ucl.ac.uk, mengya.liao@ucl.ac.uk, a.seeds@ucl.ac.uk, huiyun.liu@ucl.ac.uk).

P. P. Vasil'ev is also associated with the PN Lebedev Physical Institute, Moscow 119991, Russia.

for inexpensive lower-bandwidth lasers: for example, 10 Gb/s Ethernet Passive Optical Networks are becoming the leading technology for 5G mobile networks as well as for residential and enterprise optical access [13]. As a consequence, there is a huge potential market for low-cost QD lasers on Si if they could be demonstrated to be suitable for 10 Gb/s operation.

Yet so far, little experimental and almost no theoretical research has been undertaken on these lasers' dynamic performance [14], [15]. *Inoue et al.* have published small-signal and large-signal modulation results of InAs QD lasers on GaP/on-axis Si substrate with 3dB bandwidths of 6.5 GHz and 4.0 GHz for a *p*-doped and an undoped laser, respectively, and 12.5 Gb/s modulation [6], while 9 GHz and 31 GHz passive mode-locking have been demonstrated as well [16], [17]. In our last paper, we have reported gain-switching of Si-based QD lasers supported by numerical modeling as a first step towards a comprehensive theoretical study of the dynamics [18].

In this paper, we aim to create a deeper understanding of the intrinsic physical processes in QD lasers on Si with respect to their dynamic characteristics. For this purpose, we test narrow ridge-waveguide 1.3 µm InAs QD lasers grown on a miscut Si substrate under small-signal conditions and model the results theoretically using the three-level rate equation traveling-wave model from [18]. The extracted laser parameters are used to simulate the high-speed performance of devices in a different geometrical or epitaxial configuration, predicting maximum achievable 3dB modulation bandwidths similar to those of InAs QD lasers on GaAs in the range of 5 GHz to 7 GHz. Finally, we discuss the impact of dislocations on the dynamic performance, supporting this with numerical simulations modeling the effect of enhanced non-radiative recombination and optical losses qualitatively. We find that these do not impose a fundamental limit to the lasers' modulation speed, so that monolithic III/V QD lasers on Si optimized for communication applications should be well-suited for 10 Gb/s operation.

II. Laser Design and Static Properties

A (001) Si wafer 4 ° miscut towards the [001] axis is used as the substrate for the InAs QD laser. First, a number of buffer and defect filter layers are grown in order to minimize the number of dislocations emerging from the inherently incompatible Si-GaAs interface [19], [20]. As shown schematically in Fig. 1(a), a thin AlAs nucleation layer is grown to prevent the nucleation of three-dimensional islands, followed by a 1 µm-thick GaAs buffer layer and a dislocation filter consisting of four periods of InGaAs/GaAs strained-layer superlattices, each with 300 nm spacer layers. At this point, the dislocation density is sufficiently reduced (~10^{-5} cm^{-2}) to allow the growth of the QD laser. The III/V laser structure comprises a 1.4 µm-thick *n*-GaAs cladding layer, the undoped QD-based active region, a 1.4 µm-thick *p*-GaAs cladding layer, and a 300 nm highly *p*-doped GaAs contact layer. The five-stacked active layers each contain an InAs QD layer with an average dot density of 3 × 10^{10} cm^{-2} in an 8 nm-thin InGaAs wetting layer (WL). Consecutive dot-in-a-well structures are spaced by 50 nm GaAs barrier layers, and the entire active structure is embedded into a 140 nm GaAs waveguide. Further details can be found in [3].

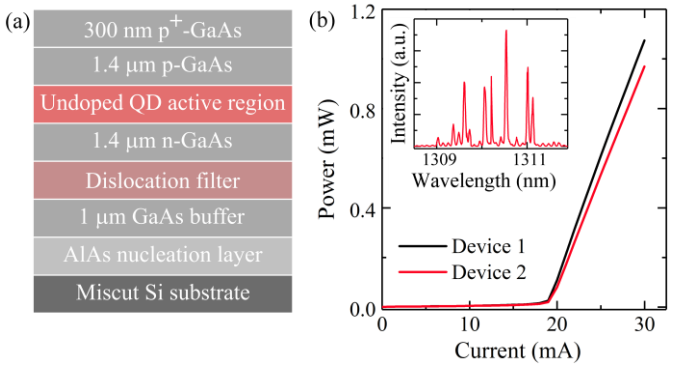

Fig. 1. (a) Schematic epitaxial structure of the InAs QD laser on a miscut Si substrate. (b) CW light-current characteristics of the tested narrow ridge-waveguide lasers at 15 °C. The multimode laser spectrum of device 2 shown in the inset is measured at a drive current of 22 mA.

2.2 µm-narrow ridge-waveguide Fabry-Pérot lasers are fabricated using standard photolithography and etching methods. The electrical *p*- and *n*-contact are formed through the deposition of Ti/Pt/Au and Ni/GeAu/Ni/Au, respectively, and an HR coating is applied to the rear facet. Finally, the thinned laser bar is mounted *p*-side up on a copper heatsink. The lasers have a cavity length of 2.5 mm, where they show good static performance. The light-current (*LI*) curves of two nominally identical lasers can be seen in Fig. 1(b), demonstrating threshold currents of 18.9 mA and 19.1 mA. The inset shows the optical spectrum just above the threshold.

III. Small-Signal Measurements and Analysis

The small-signal response of the two QD lasers is measured by probing the devices directly and imposing a swept frequency RF signal to the DC drive current. The modulated light output is collected with a singlemode fiber connected to a vector network analyzer. Fig. 2 shows the respective modulation response curves with both devices demonstrating a maximum 3dB modulation bandwidth of 1.6 GHz.

The curves are fitted using the standard three-pole transfer function [21], and the extracted damping factors γ are plotted against resonance frequency f_R, which is displayed in Fig. 3(a). A linear fit allows extraction of the *K*-factor [22], yielding

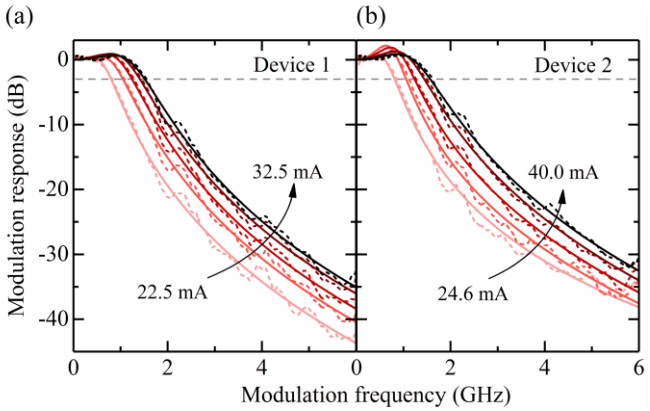

Fig. 2. Normalized and smoothed small-signal modulation response curves of the Si-based QD lasers at currents between 22.5 mA and 40 mA at 15 °C, fitted by a three-pole transfer function.

2.4 ns and 3.7 ns for device 1 and device 2, respectively. These values determine the maximum achievable 3dB bandwidth via

$$f_{3dB,max} \approx \sqrt{2} \cdot \frac{2\pi}{K} . \quad (1)$$

In the low-damping regime, f_{3dB} is usually estimated as

$$f_{3dB} \approx 1.55\, f_R = 1.55 \sqrt{\frac{v_{gr} S \partial g/\partial N}{\tau_{ph}}} \quad (2)$$

with v_{gr}, S, $\partial g/\partial N$, and τ_{ph} being the group velocity, the photon density, the differential gain, and the photon lifetime. Using (1), maximum intrinsic bandwidths of 3.7 GHz and 2.4 GHz are estimated for the tested devices [22]**.** Typical *K*-factors of InAs QD lasers on GaAs are of the order of 1 ns, and similar values of 0.92 ns and 1.3 ns have been published for the *p*-doped and the undoped Si-based QD laser, respectively, in [6]. The larger *K*-factors extracted here show that the measured small-signal curves are strongly damping limited, which is largely a result of a long photon lifetime due to low mirror losses, given as

$$\alpha_m = \frac{1}{L} \ln\left(\frac{1}{\sqrt{R_1 R_2}}\right) \quad (3)$$

with L, R_1, and R_2 being the cavity length and the facet reflectivities. Hence, it is clear that both the long cavity and the HR-coated rear facet contribute substantially to a high value of τ_{ph}, which is estimated to be about 22 ps [23]. Lasers designed for higher speed, in contrast, tend to have short cavities of a few hundred micrometers [24]-[27] – for instance the 580 µm Si-based QD laser used by *Inoue et al.* [6] – in order to keep the photon lifetime and thus the *K*-factor small. Apart from its proportionality to the photon lifetime, the *K*-factor depends, furthermore, on the differential gain and the gain compression factor [11], [28]. The simulations shown in Section V will show indeed that both quantities add to the bandwidth limitation observed in Fig. 2.

Fig. 3(b) shows f_R and f_{3dB} plotted against the square root of the current above threshold with linear fits for extraction of the *D*-factor (*D*) and the modulation current efficiency (*MCEF*), which express the rate at which f_R and f_{3dB} increase with current above threshold [21]. From Fig. 3(b) it can be seen that the *D*-factor and the *MCEF* take on values between about 0.3 GHz/mA$^{1/2}$ and 0.4 GHz/mA$^{1/2}$, which is slightly smaller than the values of about 0.7 GHz/mA$^{1/2}$ and 1.1 GHz/mA$^{1/2}$ reported in [6], but comparable with values that have been obtained during the earlier work on InAs QD lasers grown on GaAs [29], [30].

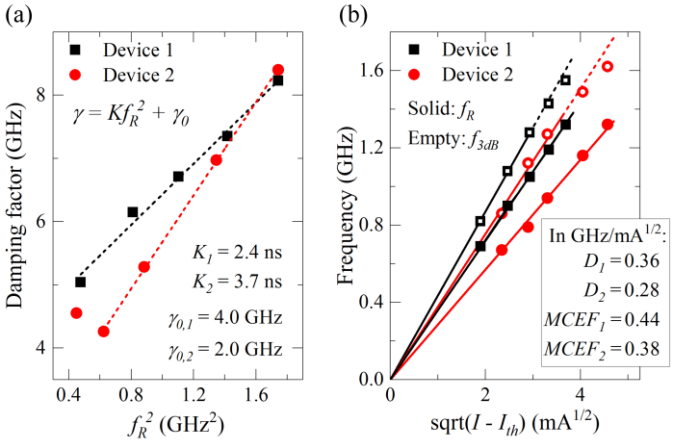

Fig. 3. (a) Damping versus squared resonance frequency for device 1 (black) and 2 (red) with linear fits. The inverse damping offset γ_0^{-1} is an estimate for the effective carrier lifetime τ, yielding τ_1 = 0.25 ns and τ_2 = 0.5 ns. (b) Resonance frequencies (solid) and 3dB frequencies (empty) versus the square root of the current above threshold with linear fits. The sublinear trends of the 3dB frequencies towards higher currents (dashed) indicate that strong damping begins to limit the modulation bandwidth.

IV. Numerical Model

The purpose of this study is less to present devices with ultra high-speed performance, but rather to identify the fundamental laser parameters through measurement and numerical modeling in order to predict the ultimately achievable speed for this particular laser structure in an adjusted laser geometry, and eventually to understand the potential limitations Si-based QD lasers encounter due to their higher dislocation densities. The traveling-wave model used for calculating these trends comprises three carrier rate equations with one-dimensional spatial resolution for calculation of the WL, excited state (ES), and ground state (GS) carrier densities. For simplicity, the following equations are limited to the computation of the electron densities rather than describing the electron and hole dynamics separately [11].

$$\frac{\partial N_{WL}}{\partial t} = \frac{\eta I}{e V_{WL}} + \frac{V_D}{V_{WL}} \frac{N_{ES}}{\tau_{esc}^{ES}} - \frac{N_{WL}(1-f_{ES})}{\tau_c} - \frac{N_{WL}}{\tau^{WL}} - D\nabla^2 N_{WL}$$

$$\frac{\partial N_{ES}}{\partial t} = \frac{V_{WL}}{V_D} \frac{N_{WL}(1-f_{ES})}{\tau_c} + \frac{N_{GS}(1-f_{ES})}{\tau_{esc}^{GS}} - \frac{N_{ES}}{\tau_{esc}^{ES}} - \frac{N_{ES}(1-f_{GS})}{\tau_0} - \frac{N_{ES}}{\tau^{ES}}$$

$$\frac{\partial N_{GS}}{\partial t} = \frac{N_{ES}(1-f_{GS})}{\tau_0} - \frac{N_{GS}(1-f_{ES})}{\tau_{esc}^{GS}} - v_{gr} g S - \frac{N_{GS}}{\tau^{GS}} . \quad (4) - (6)$$

Since this model was in part already presented in [18], the following will only provide a brief summary of the key equations. (4)-(6) describe carrier injection into the WL and diffusion into neighbouring device sections, carrier capture into the QDs and relaxation into the ground state, thermal escape, carrier losses, and finally lasing from the ground state only. An explanation of all simulation variables and parameters can be found in Table I. QD state filling or Pauli blocking, respectively, is modeled through the inclusion of ES and GS occupation probabilities f_{ES} and f_{GS}. For the calculation of the QD gain function g, the hole ground state occupation probability is set to a constant value.

The photon density S is calculated as the sum of the absolute squares of the forward and reverse propagating electric fields $E^{\pm}(z,t)$, defined by

$$\left(\frac{1}{v_{gr}}\frac{\partial}{\partial t} \pm \frac{\partial}{\partial z}\right) E^{\pm}(z,t) = (\Gamma g - \alpha_i - i\delta) E^{\pm}(z,t) + i_{sp\pm}(z,t). \quad (8)$$

(8) includes modal gain Γg, waveguide loss α_i, spontaneous noise $i_{sp\pm}$, and a detuning term δ, which takes into account chirping through Henry's alpha factor and the plasma effect from the WL carrier density [31], [32]. Finally, a Lorentzian gain filter is used to shape the spectrum acting on these fields [33].

V. Small-Signal Simulations

A. Fitting the Experimental Results

The measured *LI* characteristic and small-signal response curves are used as a fitting template for numerical modeling. While some of the used parameters are based on standard values from the literature, such as the optical confinement factor, thermal escape times, or the QD capture and intradot relaxation times, for instance, others build on values estimated in experiments (g, α_i, η) or are

known from the growth and fabrication process. The remaining unknown values are used as fitting parameters. The QD carrier lifetimes, for example, can be used to reproduce the experimental laser threshold precisely. It turns out that a slightly shorter ES and GS lifetime of 0.52 ns yields a better fit to the small-signal curves than the lifetime of 0.56 ns that allows an accurate fit of the initially measured *LI* curves, indicating that the laser may have degraded marginally in the course of performing the experiments. The extracted injection efficiency of 0.25 and the WL lifetime of 0.2 ns imply additionally that some sort of carrier loss mechanism is present. Tuning the modal gain and the gain compression factor within the boundaries imposed by the experimental *LI* characteristic is a means of adjusting the modulation bandwidth. Whereas a higher gain compression factor on the order of 10^{-15} cm^3 would reproduce the strongly damped character of the measured response curves somewhat better, it leads, however, to premature power saturation of the modeled *LI* curve, so that a value of $\varepsilon = 5 \times 10^{-16}$ cm^3 is chosen as a trade-off. The resulting small-signal simulations are displayed in Fig. 4. Apart from the fact that the numerical model overestimates the magnitude of the resonance peak slightly, the laser parameter set presented in Table I yields an excellent fit and resembles strongly a typical parameter set for the simulation of conventional InAs/GaAs QD lasers.

TABLE I
SIMULATION PARAMETERS USED FOR FIG. 4

WL and QD volume V_{WL}, V_D	Group velocity $v_{gr} = 8.4 \times 10^7$ m/s
Waveguide width $W = 2.2$ µm	Elementary charge $e = 1.6 \times 10^{-19}$ C
Number of QD layers = 5	Confinement factor $\Gamma = 7.5 \times 10^{-4}$
QD density $\rho = 2.5 \times 10^{10}$ cm^{-2}	Spontaneous emission factor $\beta = 5 \times 10^{-4}$
Gain bandwidth $\Delta\lambda = 15$ nm	GS hole occupation probability $f_{GS}^h = 0.5$
Modal gain $g_{mod} = 14.7$ cm^{-1}	Injection efficiency $\eta = 0.25$
Optical loss $\alpha_i = 3$ cm^{-1}	Diffusion constant $D = 16$ cm^2/s
Gain compression factor $\varepsilon = 5 \times 10^{-16}$ cm^3	Intradot relaxation time $\tau_0 = 150$ fs
ES, GS lifetime $\tau^{ES,GS} = 0.52$ ns	ES escape time $\tau_{esc}^{ES} = 44$ ps
WL lifetime $\tau^{WL} = 0.2$ ns	GS escape time $\tau_{esc}^{GS} = 18$ ps
Carrier capture time $\tau_c = 1$ ps	

B. *Bandwidth Optimization*

To investigate the suitability of monolithic III/V QD lasers on Si substrates for direct modulation applications, the small-signal modulation response is modeled for various laser lengths with reflectivity configurations of 0.99/0.30, 0.99/0.05, and 0.99/0.60, corresponding to HR/as-cleaved, HR/AR, and HR/HR. In addition, the impact of higher modal with twice the number of active layers is simulated [34].

The result of the simulations with an unchanged number of QD layers can be seen in Fig. 5. At first glance, the presented trends look slightly atypical, as the modulation response increases with growing cavity length and facet reflectivity, contrary to what is implied by (2). The modulation bandwidth increases for cavity lengths of up to 3.0 mm and 1.75 mm for the HR/as-cleaved and the HR/HR combination, respectively. Beyond these lengths, the 3dB frequency starts to decrease. For these scenarios, two effects come into play. Whereas both an increased laser length and higher mirror reflectivities lead to a longer photon lifetime (Fig. 6(a)), the improved optical feedback as well as the larger gain volume can enhance the photon density (Fig. 6(b)). So depending on the operation point of the laser, the net ratio of $\sqrt{S/\tau_{ph}} \propto f_R$ can increase with

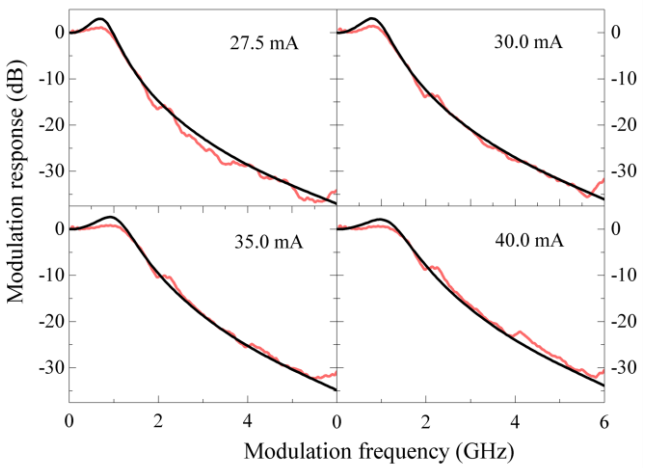

Fig. 4. Modeled (black) small-signal modulation curves of laser 2 (red) using the QD rate equation traveling-wave model with the parameters displayed in Table I and $L = 2.5$ mm, $R_1 = 0.99$, $R_2 = 0.30$.

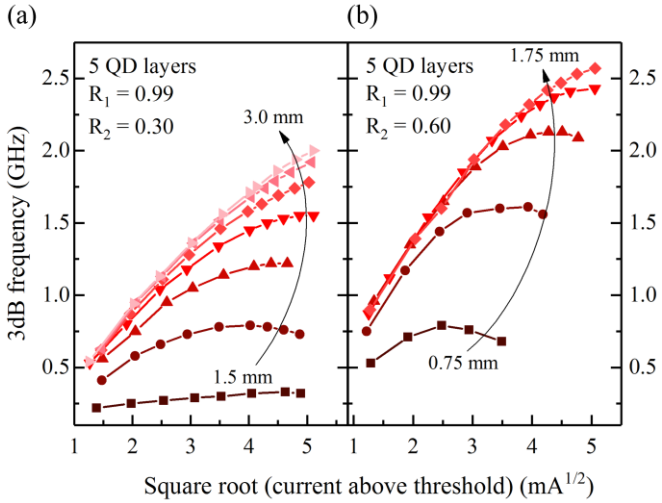

Fig. 5. 3dB frequency versus the square root of current above threshold modeled for various cavity lengths with (a) HR/as-cleaved facets ($MCEF_{max}$ = 0.49 GHz/mA$^{1/2}$) and (b) HR/HR facets ($MCEF_{max}$ = 0.67 GHz/mA$^{1/2}$). Simulations with the HR/AR configuration did not yield laser operation within the tested cavity lengths up to 4 mm.

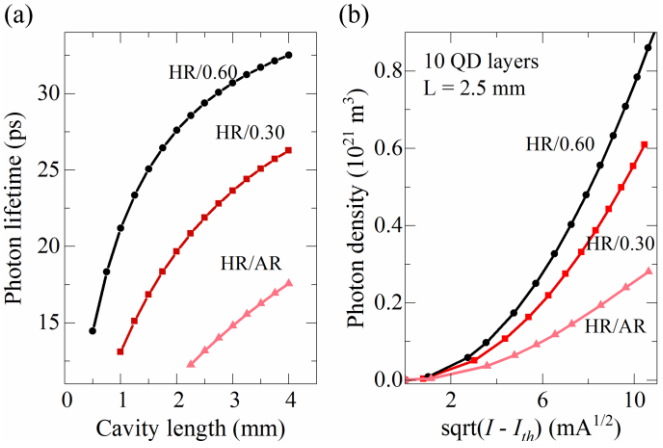

Fig. 6. (a) Photon lifetime versus cavity length calculated for three facet reflectivity combinations. (b) Modeled photon density plotted against the square root of the current above threshold for a 2.5 mm-long laser with ten active layers, illustrating the possibility of attaining higher photon densities through HR facet coatings.

increasing laser length or facet reflectivity despite the longer photon lifetime. The second effect is that the simulated lasers seem to be operated in a strongly gain-saturated regime, which often is not fully accounted for in standard analytical expressions. If insufficient gain is provided within the structure and the ratio between maximum modal gain and threshold gain is small, the effects of gain compression on the modulation response are even more pronounced [31].

The HR/HR configuration with the higher modal gain given by ten QD layers yields optimum performance for the given laser parameters with the respective results being shown in Fig. 7(a). For the 0.75 mm-short cavity, the *MCEF* is increased to 0.90 GHz/mA$^{1/2}$ and 3dB bandwidths of 3.0 GHz to 3.5 GHz are obtained. Small-signal simulations of lasers in HR/as-cleaved and HR/AR configuration yield lower maximum bandwidths of about 3.0 GHz and 2.5 GHz, respectively with the highest *MCEF*s obtained at 1.75 mm (0.67 GHz/mA$^{1/2}$) and 3.5 mm (0.42 GHz/mA$^{1/2}$). In the case of shorter cavities, the modulation bandwidth is limited by insufficient gain, while the photon lifetime is the limiting factor for longer laser lengths.

Since an increased number of QD layers usually results in a higher saturation power, the results obtained for a laser with ten QD layers in HR/HR configuration are remodeled for two lower gain compression values. The simulations in Fig. 7(b) suggest that modulation bandwidths of 5 GHz to 7 GHz, which are typical modulation speeds of InAs/GaAs QD lasers on their native substrate [24], [25], [30], [35]-[37], may be achievable on the basis of the available growth template. The modeled bandwidth is currently only limited by the gain provided from the QD active region. Simulations performed based on a high-gain active region with a high QD density, thin GaAs barrier layers, and a large confinement factor [38] promise modulation bandwidths of more than 10 GHz. The technological challenge is now to combine the growth techniques of high-quality GaAs on Si with these required for high-performance QD active regions, although the the excellent modal gain of almost 60 cm^{-1} reported in [14] proves that this does not appear to be an insurmountable hurdle.

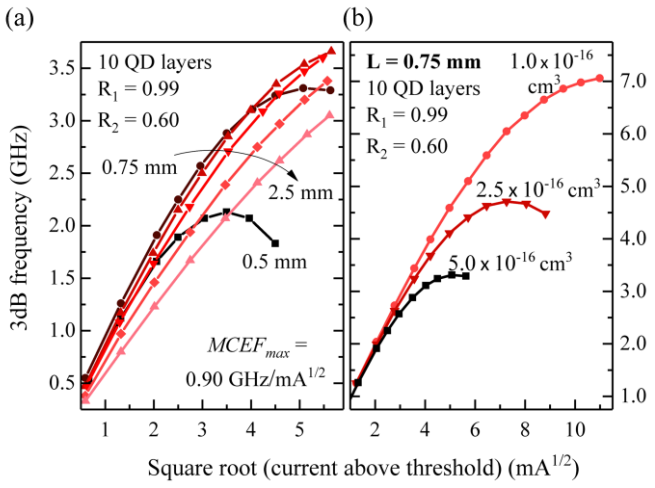

Fig. 7. (a) 3dB bandwidth versus the square root of the current above threshold modeled for various cavity lengths using ten QD layers and 99 %/60 % HR-coated facets. The confinement factor is increased by 50 % for these simulations. (b) Modulation bandwidth modeled for L = 0.75 mm using $\varepsilon = 5 \times 10^{-16}$ cm^3 as shown in Fig. 7(a) in comparison to the performance with lower gain compression factors.

VI. Discussion: Impact of the Silicon Substrate

Why exactly dislocations impair the static performance of QD lasers on Si, and why lasers with QD active regions are more immune to these effects compared with quantum wells is neither fully investigated nor completely understood. In this section, we discuss how the dynamic characteristics of a QD laser grown in Si may be affected by the problems induced by the growth on a Si substrate. While the two main points of concern are arguably carrier and optical loss induced by a high dislocation density [3], [15], [39], two further, though potentially minor factors to consider are the possibility of reduced QD uniformity caused by the enhanced surface roughness of GaAs pseudo-substrates grown on Si [4], and residual tensile stress from the mismatch of the thermal expansion coefficients of GaAs and Si [19].

Enhanced non-radiative recombination takes place as carriers from the barrier layers and WLs migrate into defect states formed by threading dislocations [15], [40]. Carriers confined in QD states, in contrast, are believed to be less affected by this loss mechanisms due to their higher confinement energy preventing them to diffuse into these states [3], [41]. The implications of this process on the modulation response can be investigated qualitatively by setting the WL lifetime τ^{WL} to a short value of 0.05 ns, representing the situation with a dislocation density much higher than in our tested lasers, and to 1.0 ns, representing the situation in a GaAs-based laser, where carrier lifetimes can be on the order of several nanoseconds [15]. The simulations in Fig. 8(a) show that the QD laser's modulation response is almost independent of τ^{WL}, with only a marginal drop observable for the τ^{WL} = 0.05 ns scenario. Hence, excess carrier loss in the WL is only of minor importance with respect to the dynamic performance given that the WL population remains sufficient to ensure population inversion in the QDs. This is an important finding, as it helps understanding why monolithic QD lasers on Si can still show laser operation even in the presence of high dislocation densities of 10^8 cm^{-2} [40]. Practically, a drastic increase of non-radiative WL recombination will require higher injection currents to supply enough carriers for the QDs, thus

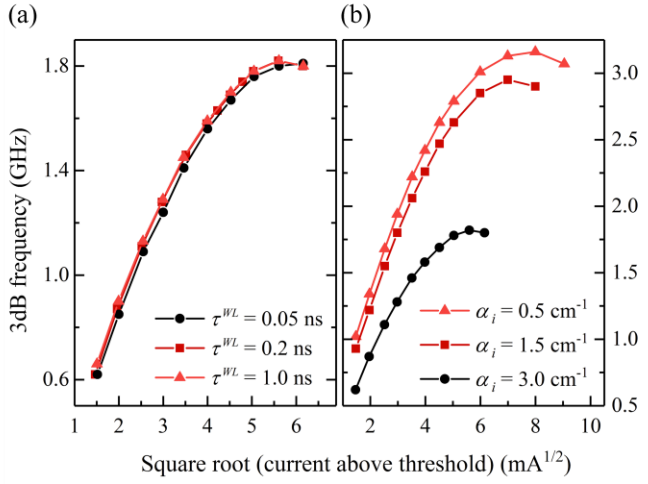

Fig. 8. 3dB frequency versus the square root of current above threshold: Impact of (a) non-radiative recombination in the WL and (b) optical loss on the modulation response of a QD laser on Si.

ultimately limiting the dislocation density at which the laser threshold can be overcome due to heating effects.

In addition to non-radiative recombination, the internal loss caused by dislocation-induced absorption and optical scattering can additionally compromise the performance of QD lasers on Si [39] – especially with respect to the modulation speed, as optical loss effectively reduces the available gain. Whereas *Wang et al.* have calculated waveguide loss on the order of 2.4 cm^{-1} to 5.5 cm^{-1} for the metamorphic epilayers of III/V QD lasers on Si in a similar configuration [39], *Shutts et al.* and *Jung et al.* have measured low internal losses of about 2.8 cm^{-1} [42] and 2.5 cm^{-1} [7], respectively, similar to what has been used in our simulations [18]. These values, even if possibly containing a residual dislocation-induced loss component, give clear evidence of the high crystal quality of the III/V lasers, and compare favorably with internal losses in QD lasers on native substrates [11], [32], This indicates that optical losses in monolithic QD lasers on Si are unlikely to limit their performance in a fundamental way. Even though reducing the optical losses further to 1.5 cm^{-1} or 0.5 cm^{-1} may almost double the modulation bandwidth in our case, as illustrated by the simulation results in Fig. 8(b), this effect is likely to be less pronounced with QD lasers on Si with higher gain.

Surface roughness can lead to increased QD inhomogeneous broadening, so that the peak modal gain may be reduced as the QD gain spreads over a wider range of energies [43]. This is also an issue for QD lasers on native substrates, whose photoluminescence (PL) spectra have a typical full-width at half-maximum (FWHM) of about 40 meV [43], [44], although much narrower FWHMs of almost 20 meV have also been demonstrated [45]. Specifically for III/V lasers on Si, the strong tensile strain resulting from the cool-down after growth can add to the issue of interlayer QD size variations [41], [44]. Yet with PL FWHMs for QDs on Si between 28 meV and 30 meV reported in [3], [5], [9], [14], and [16], as good as PL FWHMs for QDs on GaAs, improved QD growth technology seems to be able to manage the surface roughness and the tensile strain induced by the Si substrate well.

VII. Conclusion

We have presented a comprehensive study on the high-speed modulation characteristics of monolithic 1.3 µm InAs/GaAs QD lasers on Si substrate. The small-signal modulation experiments revealed maximum 3dB bandwidths of 1.6 GHz with *D*-factors of about 0.3 GHz/$mA^{1/2}$, modulation current efficiencies of 0.4 GHz/$mA^{1/2}$, and *K*-factors between 2.4 ns and 3.7 ns. Given that the tested devices have not been designed specifically for high modulation bandwidths, we have used a three-level rate equation traveling-wave model to simulate the results numerically. Based on the obtained parameter set, a theoretical design optimization study has been performed in order to predict trends for geometrical configurations yielding the fastest possible modulation response. The simulations indicate that the small-signal response is currently not only limited by the long photon lifetime, but also by low gain and high gain compression. These limitations could be overcome by increasing the number of active QD layers to ten, and by using 99 % and 60 % high-reflectivity coatings to allow for lasing at shorter cavity lengths. In this configuration, the simulations predict 3dB modulation bandwidths comparable with InAs/GaAs QD lasers on native substrates of up to 5 GHz to 7 GHz, placing Si-based QD lasers almost on a par with those grown on GaAs. Additional simulations investigating the impact of dislocations on the modulation speed reveal that neither increased non-radiative recombination through carrier migration into defect states in the wetting layer, nor dislocation-induced optical losses appear to limit the modulation characteristics in a fundamental way. This all points to the fact that researchers may well overcome the challenges of GaAs-Si heteroepitaxy successfully, and that monolithic 1.3 µm III/V QD lasers on Si have great potential – not only as monolithically embedded Si-based on-chip light source, but also for low-cost 10 Gb/s applications.

References

[1] Y. A. Vlasov, "Silicon CMOS-integrated nano-photonics for computer and data communications beyond 100G," *IEEE Commun. Mag.*, vol. 50, no. 2, pp. S67–S72, Feb. 2012.

[2] Y. Arakawa, T. Nakamura, Y. Urino, and T. Fujita, "Silicon photonics for next generation system integration platform," *IEEE Commun. Mag.*, vol. 51, no. 3, pp. 72–77, Mar. 2013.

[3] S. Chen *et al.*, "Electrically pumped continuous-wave III–V quantum dot lasers on silicon," *Nat. Photonics*, vol. 10, pp. 307–311, Mar. 2016.

[4] D. Jung, P. G. Callahan, B. Shin, K. Mukherjee, A. C. Gossard, and J. E. Bowers, "Low threading dislocation density GaAs growth on on-axis GaP/Si (001)," *J. Appl. Phys.*, vol. 122, no. 22, pp. 225703-1–225703-7, Dec. 2017.

[5] D. Jung *et al.*, "High efficiency low threshold current 1.3 µm InAs quantum dot lasers on on-axis (001) GaP/Si," *Appl. Phys. Lett.*, vol. 111, no. 12, pp. 122107, Sep. 2017.

[6] D. Inoue *et al.*, "Directly modulated 1.3 µm quantum dot lasers epitaxially grown on silicon," *Opt. Express*, vol. 26, no. 6, pp. 7022–7033, Mar. 2018.

[7] D. Jung *et al.*, "Highly reliable low-threshold InAs quantum dot lasers on on-axis (001) Si with 87% injection efficiency," *ACS Photon.*, vol. 5, no. 3, pp. 1094–1100, Dec. 2017.

[8] A. Y. Liu and J. Bowers, "Photonic integration with epitaxial III-V on Silicon," *IEEE J. Sel. Top. Quantum Electron.*, vol. 24, no. 6, pp. 6000412, Aug. 2018.

[9] J. Duan *et al.*, "Semiconductor quantum dot lasers epitaxially grown on silicon with low linewidth enhancement factor," *Appl. Phys. Lett.*, vol. 112, no. 25, pp. 251111-1–251111-4, Jun. 2018.

[10] J. Wu, S. Chen, A. J. Seeds, and H. Liu, "Quantum dot optoelectronic devices: lasers, photodetectors and solar cells," *J. Phys. D. Appl. Phys.*, vol. 48, no. 36, pp. 363001, Aug. 2015.

[11] A. Fiore and A. Markus, "Differential gain and gain compression in quantum-dot lasers," *IEEE J. Quantum Electron.*, vol. 43, no. 3, pp. 287–294, Mar. 2007.

[12] C. Cole, "Beyond 100G client optics," *IEEE Commun. Mag.*, vol. 50, no. 2, pp. S58–S66, Feb. 2012.

[13] IEEE 802.3 Ethernet Working Group, "Industry connections feasibility assessment for the next generation of EPON," 2015.

[14] Z. Zhang, D. Jung, J. C. Norman, P. Patel, W. W. Chow, and J. E. Bowers, "Effects of modulation *p* doping in InAs quantum dot lasers on silicon," *Appl. Phys. Lett.*, vol. 113, no. 6, pp. 061105-1–061105-4, Aug. 2018.

[15] H. Huang *et al.*, "Analysis of the optical feedback dynamics in InAs/GaAs quantum dot lasers directly grown on silicon," *JOSA B*, vol. 35, no. 11, pp. 2780–2787, Nov. 2018.

[16] S. Liu, J. C. Norman, D. Jung, MJ Kennedy, A. C. Gossard, and J. E. Bowers, "Monolithic 9 GHz passively mode locked quantum dot lasers directly grown on on-axis (001) Si," Appl. Phys. Lett., vol. 113, no. 4, pp. 041108-1–041108-4, Jul. 2018.

[17] S. Liu, D. Jung, J. C. Norman, M. J. Kennedy, A. C. Gossard, and J. E. Bowers, "490 fs pulse generation from passively mode-locked single

section quantum dot laser directly grown on on-axis GaP/Si," *Electron. Lett.*, vol. 54, no. 7, pp 432–433, Apr. 2018.

[18] C. Hantschmann *et al.*, "Gain switching of monolithic 1.3 μm InAs/GaAs quantum dot lasers on silicon," *J. Lightw. Technol.*, vol. 36, no. 18, pp. 3837–3842, Sep. 2018.

[19] A. Georgakilas, P. Panayotatos, J. Stoemenos, J.-L. Mourrain, and A. Christou, "Achievements and limitations in optimized GaAs films grown on Si by molecular-beam epitaxy," *J. App. Phys.*, vol. 71, no. 6, pp. 2679–2701, Mar. 1992.

[20] S.-H. Choi, R. Ai, and S. A. Barnett, "Suppression of three-dimensional island and nucleation during GaAs growth on Si(001)," *Phys. Rev. Lett.*, vol. 67, no. 20, pp. 2826–2829, Nov. 1991.

[21] A. Larsson, C. Carlsson, J. Gustavsson, Å. Haglund, P. Modh, and J. Bengtsson, "Direct high-frequency modulation of VCSELs and applications in fibre optic RF and microwave links," *New J. Phys.*, vol. 6, no. 1, pp. 176, Nov. 2004.

[22] L. A. Coldren, S. W. Corzine, and M. L. Mashanovitch, "Dynamic effects," in *Diode Lasers and Photonic Integrated Circuits*, New York, NY, USA: John Wiley & Sons, 2012, pp. 185–261.

[23] P. P. Vasil'ev, "Gain and q-switching in diode lasers," in *Ultrafast Diode Lasers – Fundamentals and Applications*, Norwood, MA, USA: Artech House, 1995, pp. 53–93.

[24] M. Kuntz *et al.*, "10 Gbit/s data modulation using 1.3 μm InGaAs quantum dot lasers," *Electron. Lett.*, vol. 41, no. 5, pp. 244–245, Mar. 2005.

[25] K. Otsubo *et al.*, "Temperature-insensitive eye-opening under 10-Gb/s modulation of 1.3-μm p-doped quantum-dot lasers without current adjustments," *Jpn. J. Appl. Phys.*, vol. 43, no. 8B, pp. L1124–L1126, Aug. 2004.

[26] S. Fathpour, Z. Mi, and P. Bhattacharya, "Small-signal modulation characteristics of p-doped 1.1- and 1.3-μm quantum-dot lasers," *IEEE Photon. Technol. Lett.*, vol. 17, no. 11, pp. 2250–2252, Nov. 2005.

[27] M. Ishida et al., "Temperature-stable 25-Gbps direct-modulation in 1.3-μm InAs/GaAs quantum dot lasers," in *Proc. Conf. Lasers Electro-Opt. Conf. Quantum Electron. Laser Sci.*, San Jose, CA, USA, 2012, p. Cm1I.2.

[28] A. E. Zhukov, M. V. Maksimov, and A. R. Kovsh, "Device characteristics of long-wavelength lasers based on self-organized quantum dots," *Semiconductors*, vol. 46, no. 10, pp. 1249–1273, Oct. 2012.

[29] K. Kamath, J Phillips, H. Jiang, J. Singh, and P. Bhattacharya, "Small-signal modulation and differential gain of single-mode self-organized $In_{0.4}Ga_{0.6}As$/GaAs quantum dot lasers," *Appl. Phys. Lett.*, vol. 70, no. 22, pp. 2952–2953, Jun. 1997.

[30] R. Krebs, F. Klopf, S. Rennon, J. P. Reithmaier, and A. Forchel, "High frequency characteristics of InAs/GaInAs quantum dot distributed feedback lasers emitting at 1.3 μm," *Electron. Lett.*, vol. 37, no. 20, pp. 1223–1225, Sep. 2001.

[31] F. Grillot, B. Dagens, J.-G. Provost, H. Su, and L. F. Lester, "Gain compression and above-threshold linewidth enhancement factor in 1.3-μm InAs-GaAs quantum-Dot lasers," *IEEE J. Quantum Electron.*, vol. 44, no. 10, pp. 946–951, Oct. 2008.

[32] M. Gioannini, A. Sevega, and I. Montrosset, "Simulations of differential gain and linewidth enhancement factor of quantum dot semiconductor lasers," *Opt. Quant. Electron.*, vol. 38, no. 4-6, pp. 391–394, Mar. 2006.

[33] M. Thompson, "Ultra-short pulse generation in quantum well and quantum dot monolithic mode-locked laser diodes," Ph.D. dissertation, Dept. Eng., University of Cambridge, Cambridge, UK, 2006.

[34] M. Grundmann and D. Bimberg, "Gain and threshold of quantum dot lasers: theory and comparison to experiments," *Jpn. J. Appl. Phys.*, vol. 36, no. 6B, pp. 4181–4187, Jun. 1997.

[35] M. Kuntz *et al.*, "Direct modulation and mode locking of 1.3 μm quantum dot lasers," *New J. Phys.*, vol. 6, no. 1, pp. 181-1–181-11, Nov. 2004.

[36] M. Laemmlin *et al.*, "Quantum dot based photonic devices at 1.3 μm: Direct modulation, mode-locking, SOAs and VCSELs," *Phys. Stat. Sol. (c)*, vol. 3, no. 3, pp. 391–394, Feb. 2006.

[37] D. Arsenijević and D. Bimberg, "Quantum-dot lasers for 35 Gbit/s pulse-amplitude modulation and 160 Gbit/s differential quadrature phase-shift keying," in *Proc. SPIE Vol. 9892*, Brussels, Belgium, 2016, pp. 98920S.

[38] T. Kageyama *et al.*, "Large modulation bandwidth (13.1 GHz) of 1.3 μm-range quantum dot lasers with high dot density and thin barrier layer," *Proc. CSW*, Toyama, Japan, 2016, p. MoC3-4

[39] J. Wang *et al.*, "Optimization of 1.3 μm InAs/GaAs quantum dot lasers epitaxially grown on silicon: taking the optical loss of metamorphic epilayers into account," *Laser Phys.*, vol. 28, no. 12, pp. 126206, Oct. 2018.

[40] D. Jung *et al.*, "Impact of threading dislocation density on the lifetime of InAs quantum dot lasers on Si," *Appl. Phys. Lett.*, vol. 112, no. 15, pp. 153507-1–153507-4, Apr. 2018.

[41] B. Kunert, Y. Mols, M. Baryshniskova, N. Waldron, A. Schulze, and R. Langer, "How to control defect formation in monolithic III/V hetero-epitaxy on (001) Si? A critical review on current approaches," *Semicond. Sci. Technol.*, vol. 33, no. 9, pp. 093002, Aug. 2018.

[42] S. Shutts *et al.*, "Degradation studies of InAs/GaAs QD lasers grown on Si," *Proc. IEEE ISLC*, Santa Fe, NM, USA, 2018.

[43] H. Y. Liu *et al.*, "Improved performance of 1.3 μm multilayer InAs quantum-dot lasers using a high-growth-temperature GaAs spacer layer," *Appl. Phys. Lett.*, vol. 85, no. 5, pp. 704–706, Aug. 2004.

[44] K. Nishi, H. Saito, S. Sugou, and J.-S. Lee, "A narrow photoluminescence linewidth of 21 meV at 1.35 μm from strain-reduced InAs quantum dots covered by $In_{0.2}Ga_{0.8}As$ grown on GaAs substrates, *Appl. Phys. Lett.*, vol. 74, no. 8, pp. 1111–113, Feb. 1999.

[45] E. C. Le Ru, A. J. Bennett, C. Roberts, and R. Murray, "Strain and electronic interactions in InAs/GaAs quantum dot multilayers for 1300 nm emission," *Appl. Phys. Lett.*, vol. 91, no. 3, pp. 1365–1370, Feb. 2002.